

Generating Merger Trees for Dark Matter Haloes: A Comparison of Methods

Arthur Fangzhou Jiang^{*} & Frank C. van den Bosch

Department of Astronomy, Yale University, New Haven, CT 06511, USA

ABSTRACT

Halo merger trees describe the hierarchical mass assembly of dark matter haloes, and are the backbone for modeling galaxy formation and evolution. Merger trees constructed using Monte Carlo algorithms based on the extended Press-Schechter (EPS) formalism are complementary to those extracted from N-body simulations, and have the advantage that they are not trammled by limited numerical resolution and uncertainties in identifying (sub)haloes and linking them between snapshots. This paper compares multiple EPS-based merger tree algorithms to simulation results using four diagnostics: progenitor mass function (PMF), mass assembly history (MAH), merger rate per descendant halo, and the unevolved subhalo mass function (USMF). In general, algorithms based on spherical collapse yield major-merger rates that are too high by a factor of two, resulting in MAHs that are systematically offset. Assuming ellipsoidal collapse solves most of these issues, but the particular algorithm investigated here that incorporates ellipsoidal collapse dramatically overpredicts the minor-merger rate for massive haloes. The only algorithm in our comparison that yields MAHs, merger rates, and USMFs in good agreement with simulations, is that by Parkinson et al. (2008). However, this is not a true EPS-based algorithm as it draws its progenitor masses from a PMF calibrated against simulations, rather than ‘predicted’ by EPS. Finally we emphasize that the benchmarks used to test the EPS algorithms are obtained from simulations and are hampered by significant uncertainties themselves. In particular, MAHs and halo merger rates obtained from simulations by different authors reveal discrepancies that easily exceed 50 percent, even when based on the same simulation. Given this status quo, merger trees constructed using the Parkinson et al. algorithm are as accurate as those extracted from N-body simulations.

Key words: methods: analytical — methods: statistical — galaxies: haloes — dark matter

1 INTRODUCTION

Halo merger trees describe the hierarchical mass assembly of dark matter haloes. They are the backbone for modeling the formation and evolution of galaxies (see Mo, van den Bosch & White 2010), and they are the core ingredient in semi-analytical models that aim to describe the substructure of dark matter haloes (e.g., Oguri & Lee 2004; Zentner et al. 2005; Taylor & Babul 2005a,b; van den Bosch et al. 2005; Gan et al. 2010). Two different methods are used to construct halo merger trees: Monte Carlo methods based on the extended Press-Schechter (EPS; Bond et al. 1991) formalism and numerical N -body simulations. Although the rapid advances in computer technology has shifted focus from EPS-based merger trees to extracting merger trees from numer-

ical simulations (e.g., Kauffmann et al. 1999a,b; Benson et al. 2000; Helly et al. 2003; Kang et al. 2005; Springel et al. 2005; Han et al. 2012; Behroozi et al. 2013), EPS-based methods remain an important and powerful alternative for a number of reasons.

First of all, EPS methods are typically much faster and more flexible. Although a cosmological simulation typically yields merger trees (after analysis) of thousands of haloes at once, whereas an EPS-based method constructs halo merger trees for each halo at a time, the limited force resolution and mass resolution of N-body simulations introduce serious systematics. In particular, the merger trees of more massive haloes are better resolved, i.e., probe down to progenitor masses that are a smaller fraction of the mass of the final host halo. This complicates a proper analysis of how the (statistical) properties of merger trees scale with halo mass.

Furthermore, to explore the dependence on cosmological parameters typically requires one to run large sets of

^{*} E-mail:fangzhou.jiang@yale.edu

simulations. The EPS-based method, on the other hand, can typically construct halo merger trees at high mass resolution (i.e., down to progenitors with a mass as small as 10^{-5} times that of the final host halo mass) in a matter of seconds, and can therefore construct merger trees for large sets of haloes of different masses and/or cosmologies in a fraction of the time required to run and analyze a full blown cosmological simulation.

In addition, it is important to realize that although simulations more reliably capture the physics of gravitational collapse and halo growth in a hierarchical universe than EPS theory, extracting reliable merger trees from simulations is subject to a large number of tricky, systematic issues. In particular, depending on the algorithms used to identify haloes and subhaloes, and to link haloes between different snapshots, one can obtain merger trees that differ substantially (e.g., Harker et al. 2006; Fakhouri & Ma 2008, 2009; Fakhouri et al. 2010; Genel et al. 2008, 2009, 2010). Indeed, a recent comparison of ten different merger tree construction algorithms applied to the same simulation output has revealed a discomfoting amount of disparity (Srisawat et al. 2013).

In this paper, we compare a number of different methods, available in the literature, that are used to construct EPS-based merger trees. These cover a variety of strategies: some algorithms make the implicit assumption that each branching point in the tree represents a binary merger, while others allow for multiple mergers per branching point; some algorithms assure that the sum of the progenitor mass exactly equals the mass of the descendant, while others admit mild violation of mass conservation; some algorithms are based on the (standard) spherical collapse model, while others adopt the more realistic picture of ellipsoidal collapse; and finally, some algorithms are self-consistent, while others use a progenitor mass function that is inconsistent with EPS. By comparing with numerical simulations, we test how accurately these methods can reproduce various statistics of the hierarchical assembly of dark matter haloes, such as the unevolved subhalo mass function (i.e., the mass function of subhaloes at accretion), merger rates, and mass assembly histories.

This paper is organized as follows: §2 discusses the anatomy of merger trees, and the challenges associated with their construction using either numerical simulations or semi-analytical methods based on the excursion set formalism. §3 describes the various merger tree algorithms that are tested and compared in terms of their progenitor mass functions (§4.1), mass assembly histories (§4.2), merger rates per descendant halo (§4.3) and their unevolved subhalo mass functions (§4.4). Results are summarized in §5.

2 HALO MERGER TREES

2.1 Anatomy of a Merger Tree

Before describing how to construct halo merger trees using the EPS formalism, we first define some terminology used throughout this paper. Fig. 1 shows a schematic representation of a merger tree illustrating its anatomy. We refer to the halo at the base of the tree (i.e., the large purple halo at $z = z_0$) as the *host halo*. For each individual branching

point along the tree (one example is highlighted in Fig. 1), the end-product of the merger event is called the *descendant halo*, while the haloes that merge are called the *progenitors*. The *main progenitor* of a descendant halo is the progenitor that contributes the most mass. For example, for the branching point highlighted in Fig. 1, the purple halo at $z = z_2$ is the main progenitor of its descendant at $z = z_1$. The *main branch* of the merger tree is defined as the branch tracing the main progenitor of the main progenitor of the main progenitor, etc. (i.e., the branch connecting the purple haloes). Note, that the main progenitor halo at redshift z is not necessarily the most massive progenitor at that redshift. Throughout we shall occasionally refer to the main progenitor haloes of a given host halo as its zeroth-order progenitors, while the mass history, $M(z)$, along this branch is called the *mass assembly history* (MAH). Haloes that accrete directly onto the main branch are called first-order progenitors, or, after accretion, first-order subhaloes. Similarly, haloes that accrete directly onto first-order progenitors are called second-order progenitors, and they end up at $z = z_0$ as second-order subhaloes (or sub-subhaloes) of the host halo. The same logic is used to define higher-order progenitors and subhaloes, as illustrated in Fig. 1. Note that with our definition, the mass of a n^{th} -order subhalo *includes* the masses of its own subhaloes (i.e., those of order larger than n). Finally, the small shaded boxes present at each branching reflect the mass accreted by the descendant halo in the form of smooth accretion (i.e., not part of any halo) or in the form of progenitor haloes with masses below the mass resolution of the merger tree. Throughout this paper we shall refer to this component as *smooth accretion*.

2.2 Merger Trees based on EPS formalism

The extended Press-Schechter (EPS) formalism, also known as the excursion-set formalism, developed by Bond et al. (1991) and Bower (1991), uses the statistics of Gaussian random fields to compute the conditional probability $P(M_1, z_1 | M_0, z_0) dM_1$, that a halo of mass M_0 at redshift z_0 has a progenitor with mass in the range $[M_1, M_1 + dM_1]$ at redshift $z_1 > z_0$. This conditional probability function is the basis from which one can construct an (EPS-based) halo merger tree.

Following Lacey & Cole (1993), we use the variables $S \equiv \sigma^2(M)$ and $\omega \equiv \delta_c(z)$ to label mass and redshift, respectively. Here $\sigma^2(M)$ is the variance of the density field, linearly extrapolated to $z = 0$ and smoothed with a sharp k -space filter of mass M , and $\delta_c(z)$ is the critical overdensity for collapse at redshift z . In the case of spherical collapse, $\delta_c(z) = 1.686/D(z)$ with $D(z)$ the linear growth rate normalized to unity at $z = 0$. According to the EPS formalism, the conditional probability function $P(M_1, z_1 | M_0, z_0)$ is given by

$$P(M_1, z_1 | M_0, z_0) = f_{\text{SC}}(S_1, \omega_1 | S_0, \omega_0) \left| \frac{dS_1}{dM_1} \right|, \quad (1)$$

where $S_i = S(M_i)$, $\omega_i = \omega(z_i)$, and

$$f_{\text{SC}}(S_1, \omega_1 | S_0, \omega_0) = \frac{1}{\sqrt{2\pi}} \frac{\Delta\omega}{\Delta S^{3/2}} \exp\left(-\frac{\Delta\omega^2}{2\Delta S}\right), \quad (2)$$

with $\Delta S \equiv S_1 - S_0$ and $\Delta\omega = \omega_1 - \omega_0$. The progenitor mass function (hereafter PMF) at $z = z_1$ for a host halo of mass

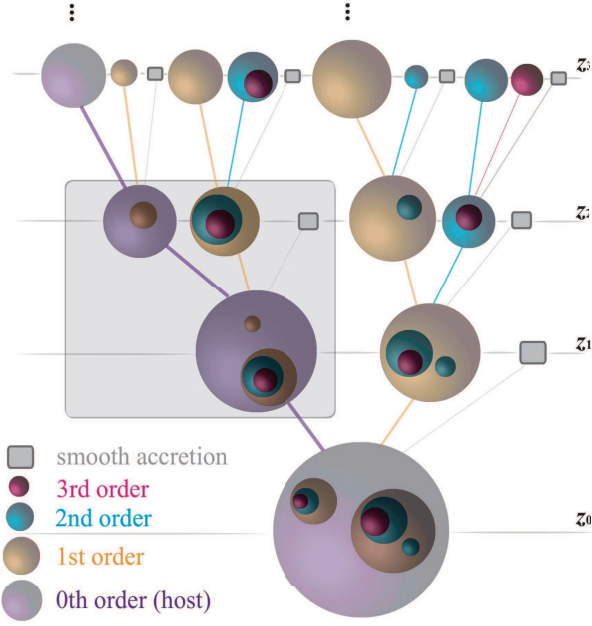


Figure 1. Illustration depicting the anatomy of a merger tree for a host halo (purple sphere at the bottom) at redshift $z = z_0$. The purple spheres to the left illustrate the assembly history of the main progenitor. We refer to these as ‘zeroth-order’ progenitors, and they accrete ‘first-order’ progenitors, which end up as (first-order) subhaloes at $z = z_0$. In turn, these first-order progenitors accrete second-order progenitors which end-up as second-order subhaloes (sub-subhaloes) at $z = z_0$, etc. The size of a sphere is proportional to its mass, while its color reflects its order, as indicated. The large, shaded box highlights a single branching point in the tree structure, which shows a descendant halo plus its single-time-step progenitors. This is the building block of an EPS merger tree. The small shaded boxes present at each branching point reflect ‘smooth accretion’, as defined in the text.

M_0 at z_0 is simply related to the mass-weighted conditional probability function by

$$n_{\text{EPS}}(M_1, z_1 | M_0, z_0) dM_1 = \frac{M_0}{M_1} P(M_1, z_1 | M_0, z_0) dM_1. \quad (3)$$

Note that the PMF $n_{\text{EPS}}(M_1, z_1 | M_0, z_0)$ is also sometimes denoted as $dN(M_1, z_1 | M_0, z_0) / dM_1$, in that $n_{\text{EPS}}(M_1, z_1 | M_0, z_0) dM_1$ is the ensemble average number $dN(M_1, z_1 | M_0, z_0)$ that a halo of mass M_0 at redshift z_0 has a progenitor with mass in $[M_1, M_1 + dM_1]$ at redshift $z_1 > z_0$. In the case of ellipsoidal collapse, the same formalism can be used, but with f_{SC} replaced by

$$f_{\text{EC}}(S_1, \omega_1 | S_0, \omega_0) = \frac{A_0}{\sqrt{2\pi}} \frac{\Delta\omega}{\Delta S^{3/2}} \exp\left(-\frac{A_1^2}{2} \tilde{S}\right) \times \left\{ \exp\left(-A_3 \frac{\Delta\omega^2}{2\Delta S}\right) + A_2 \tilde{S}^{3/2} \left[1 + 2A_1 \sqrt{\frac{\tilde{S}}{\pi}} \right] \right\}, \quad (4)$$

where $A_0 = 0.8661(1 - 0.133\nu_0^{-0.615})$, $A_1 = 0.308\nu_0^{-0.115}$, $A_2 = 0.0373\nu_0^{-0.115}$, $A_3 = A_0^2 + 2A_0A_1\sqrt{\Delta S \tilde{S}} / \Delta\omega$, $\nu_0 = \omega_0^2 / S_0$, and $\tilde{S} = \Delta S / S_0$ (see Zhang et al. 2008a,b for details).

In order to construct an EPS merger tree, one starts from some target host halo mass, M_0 , at some redshift z_0 , and uses the PMF to draw a set of progenitor masses

M_1, M_2, \dots, M_{N_p} at some earlier time $z_1 = z_0 + \Delta z$, where $\sum_{i=1}^{N_p} M_i = M_0$ in order to assure mass conservation. The time-step Δz used sets the ‘temporal resolution’ of the merger tree. This procedure is then repeated for each progenitor with mass $M_i > M_{\text{res}}$, thus advancing ‘upwards’ along the tree. The minimum mass M_{res} sets the ‘mass resolution’ of the merger tree and is typically expressed as a fraction of the final host mass M_0 .

There are two problems with this approach. First of all, although EPS provides the PMF, it does not explicitly specify how to split descendants into progenitors. In fact, this can be done using many different ways, resulting in merger trees with different statistics. Secondly, the EPS formalism is at best a crude approximation, and the PMF that it predicts may not be sufficiently accurate to yield reliable merger trees. We now discuss each of these two issues in turn.

2.2.1 The Self-consistency Constraint

The requirement for mass conservation implies that the probability for the mass of the n^{th} progenitor of some descendant needs to be conditional on the masses of the $n - 1$ progenitor haloes already drawn. Unfortunately, these conditional probability functions are not derivable from the EPS formalism, which results in ambiguity as to how to partition the descendant mass into progenitor masses. This has resulted in the construction of a variety of different Monte Carlo algorithms to construct halo merger trees within the same EPS framework, i.e., relying on the same $n_{\text{EPS}}(M_1, z_1 | M_0, z_0)$.

In order to be consistent with EPS, it is crucial that the Monte Carlo algorithm used to construct the merger trees *exactly* reproduces the EPS conditional mass function $n_{\text{EPS}}(M_1, z_1 | M_0, z_0)$ for a single time step $\Delta z = z_1 - z_0$. As shown by Zhang et al. (2008b), this is a sufficient condition for the algorithm to also reproduce the $n_{\text{EPS}}(M, z | M_0, z_0)$ for *any* z , regardless of the number, or width, of intervening time-steps. We shall refer to this as the self-consistency requirement for the Monte Carlo algorithm.

Several Monte-Carlo merger-tree algorithms rely on the assumption that in the limit of sufficiently small time-steps, all mergers are binary in nature (e.g., Cole 1991; Lacey & Cole 1993; Cole et al. 2000; Moreno, Giocoli & Sheth 2008). Under this assumption it is trivial to assign the progenitor masses using the constraint of mass conservation; after drawing the first progenitor mass, M_1 , from $n_{\text{EPS}}(M_1, z_1 | M_0, z_0)$ the mass of the second progenitor is simply $M_2 = M_0 - M_1$. An implicit assumption of this binary method is that the PMF is symmetric, such that $n_{\text{EPS}}(M_1, z_1 | M_0, z_0) = n_{\text{EPS}}(M_0 - M_1, z_1 | M_0, z_0)$. However, as shown by Sheth & Pitman (1997), this is only correct for Poisson initial conditions ($P(k) = k^n$ with $n = 0$). For more relevant cases, such as CDM, $n_{\text{EPS}}(M_1, z_1 | M_0, z_0)$ is (slightly) asymmetric, even in the limit $\Delta z \rightarrow 0$.[†] Consequently, all binary methods violate the self-consistency constraint. Cole et al. (2000) tried to remedy this by explicitly accounting for accretion of objects below the mass resolution, M_{res} , of the merger tree. However, as shown in Zhang

[†] This also implies that the assumption of binary mergers is incorrect, even in the limit $\Delta z \rightarrow 0$ (see Neistein & Dekel 2008b).

et al. (2008b) this method still violates the self-consistency constraint, albeit at a much reduced level (see §4.1 below).

In order to overcome these problems, several algorithms have been developed that do not make the implicit assumption of binarity (e.g., Kauffmann & White 1993; Sheth & Lemson 1999; Somerville & Kolatt 1999; Zhang et al. 2008b; Neistein & Dekel 2008b). Among these, only the methods of Kauffmann & White (1993; hereafter KW93), Zhang et al. (2008b), and Neistein & Dekel (2008b) fulfill the self-consistency requirement. The method of Sheth & Lemson (1999) is only exact for Poisson initial conditions, while the method of Somerville & Kolatt (1999) violates self-consistency, because it discards progenitors drawn from the conditional mass function that overflow the mass budget (see §3.1 below).

2.2.2 Beyond Spherical Collapse

In addition to problems related to the self-consistency constraint, EPS-based merger trees are also hampered by the fact that EPS is an approximate theory at best. This implies that the PMF, $n_{\text{EPS}}(M_1, z_1 | M_0, z_0)$, obtained using EPS theory, may not be sufficiently accurate. Indeed, comparison with numerical simulations has shown that the EPS conditional mass function based on the assumptions of spherical collapse overpredicts (underpredicts) the number of low-mass (massive) progenitors (Cole et al. 2008). Related to this is the well-known problem that EPS predicts halo assembly to occur later than what is found in numerical simulations (e.g., van den Bosch 2002; Lin, Jing & Lin 2003; Neistein et al. 2006).

These problems seem to be related to the assumption that halo collapse is a spherical process. Several studies have shown that assuming ellipsoidal, rather than spherical, collapse conditions, results in overall halo mass functions and halo formation times in better agreement with numerical simulations (e.g., Sheth, Mo & Tormen 2001; Hiodelis & Del Popolo 2006; Giocoli et al. 2007). In the excursion set approach, the problem of estimating halo abundances reduces to that of computing the number of time steps a Brownian-motion random walk must take before it crosses an overdensity barrier. In the spherical collapse (SC) picture, this barrier has a constant height (i.e., the critical overdensity for collapse is independent of mass scale), allowing one to calculate the up-crossing statistics for a Gaussian random field analytically. In the case of ellipsoidal collapse (EC), however, the constant barrier needs to be replaced with a ‘moving barrier’, i.e., a barrier that depends on mass scale (see Mo et al. 2010 for details). Based on the success of EC in predicting the *unconditional* halo mass function, a number of algorithms have been developed that use the PMF derived under EC conditions. Moreno et al. (2008) approximate the up-crossing barrier as being proportional to the square root $\sigma(M)$ of the mass variance, in which case the conditional mass function can be obtained analytically. Unfortunately, this barrier shape is different from the one predicted based on EC considerations (Sheth & Tormen 2002). In addition, the Moreno et al. merger-tree algorithm assumes binary mergers, resulting in a violation of the self-consistency algorithm. Zhang et al. (2008a) computed the PMF under ellipsoidal collapse conditions using a more general barrier shape, and showed that it agrees closely with the

exact, but computationally expensive, method developed by Zhang & Hui (2006). Zhang et al. (2008b) then used this EC PMF, given by Eqs. (1), (3) and (4), to develop a number of different merger-tree algorithms, some of which we will discuss and test in this paper.

Although the EC assumptions generally yields EPS predictions in better agreement with simulations, significant discrepancies remain (e.g., Sheth & Tormen 2002; Zhang et al. 2008a; Cole et al. 2008). This has prompted a number of studies to develop merger tree algorithms that use progenitor mass functions calibrated to match certain N -body simulations (Neistein & Dekel 2008a; Cole et al. 2008; Parkinson et al. 2008). These methods basically side-step EPS, but instead inherit all the problems related to subhalo identification and limitations due to finite mass resolution discussed above.

3 MERGER TREE ALGORITHMS

The main goal of this paper is to assess the performances, compared to numerical simulations, of a number of merger tree algorithms regarding a variety of statistics. In this section we briefly describe the various merger tree algorithms that enter our comparison. These are the ‘N-branch method with accretion’ method developed by Somerville & Kolatt (1999; hereafter SK99), the binary method of Cole et al. (2000; hereafter C00) and its modification by Parkinson et al. (2008; hereafter P08), and several of the algorithms suggested by Zhang et al. (2008b; hereafter Z08). What follows is a description of how these different algorithms select progenitor haloes for a single descendant halo, which constitutes the building block of a merger tree.

3.1 Somerville & Kolatt (1999)

Somerville & Kolatt (1999) developed a merger-tree algorithm that does not make the assumption of binary mergers. Their ‘N-branch method with accretion’ allows for an arbitrary number of progenitors per time-step, and has been widely used, especially in analytical models for the population of dark matter subhaloes (see Jiang & van den Bosch 2014). The algorithm is based on drawing progenitor masses from the (mass-weighted) conditional mass function. With each new halo drawn it is checked whether the sum of the progenitor masses exceeds the mass of the descendant. If this is the case the progenitor is rejected and a new progenitor mass is drawn. Any progenitor with mass $M < M_{\text{res}}$ is added to the smooth accretion component M_{smooth} (i.e., the formation history of these small mass progenitors is not followed further back in time). This procedure is repeated until the total mass left ($M - M_{\text{smooth}} - \sum M_i$) is less than M_{res} . This remaining mass is assigned to M_{smooth} .

3.2 Cole et al. (2000)

The method of Cole et al. (2000; hereafter C00) is an improvement over the ‘block model’ developed by Cole et al. (1994) and can be described as a binary method with (fixed) accretion. Similar to SK99, it treats the mass in progenitors below the mass resolution, M_{res} , as accreted mass. However, unlike SK99, the smooth accretion mass for

a given time step is deterministic, calculated by integrating the mass-weighted conditional mass function, i.e.,

$$M_{\text{smooth}}(z_1 \rightarrow z_0) = \int_0^{M_{\text{res}}} n_{\text{EPS}}(M_1, z_1 | M_0, z_0) M_1 dM_1, \quad (5)$$

where M_0 is the descendant mass. For each branching point, it is first decided how many progenitors the descendant has by calculating the mean number of progenitor haloes in the mass range $[M_{\text{res}}, M_0/2]$, given by

$$\mathcal{P} \equiv \int_{M_{\text{res}}}^{M_0/2} n_{\text{EPS}}(M_1, z_1 | M_0, z_0) dM_1. \quad (6)$$

The merger tree time steps, $\Delta\omega$, are chosen such that $\mathcal{P} \ll 1$, to ensure that multiple fragmentation is unlikely. A random number, \mathcal{R} , generated in the interval $[0, 1]$, is used to determine whether the descendant has one ($\mathcal{R} > \mathcal{P}$) or two progenitors ($\mathcal{R} \leq \mathcal{P}$). In the case of a single progenitor, its mass is $M_1 = M_0 - M_{\text{acc}}$. In the case of two progenitors, one progenitor mass, M_1 , is drawn from the progenitor mass function $n_{\text{EPS}}(M_1, z_1 | M_0, z_0)$ in the range $[M_{\text{res}}, M_0/2]$, and the second progenitor is assigned a mass $M_2 = M_0 - M_1 - M_{\text{res}}$.

3.3 Parkinson et al. (2008)

Parkinson et al. (2008; hereafter P08) modified the C00 algorithm by using a progenitor mass function tuned to match results from the Millennium Simulation (Springel et al. 2005), rather than the EPS progenitor mass function. Specifically, they used the PMF

$$n(M_1, z_1 | M_0, z_0) \equiv n_{\text{EPS}}(M_1, z_1 | M_0, z_0) G(S_1/S_0, \omega_0^2/S_0), \quad (7)$$

where $G(S_1/S_0, \omega_0^2/S_0)$ is a perturbing function that is tuned to match simulation results. P08 adopted the functional form

$$G(S_1/S_0, \omega_0^2/S_0) = G_0 \left(\frac{S_1}{S_0} \right)^{\gamma_1} \left(\frac{\omega_0^2}{S_0} \right)^{\gamma_2}, \quad (8)$$

which has the advantage that the two terms G_0 and $(\omega_0^2/S_0)^{\gamma_2}$ only enter the integral equations for M_{smooth} and \mathcal{P} (eqs. [5] and [6], respectively) as multiplicative constants. Using merger trees constructed from the Millennium Simulation by Cole et al. (2008), based on Friends-of-Friends (FoF) groups, P08 inferred the following best-fit values for the free parameters of their perturbing function: $G_0 = 0.57$, $\gamma_1 = 0.19$ and $\gamma_2 = -0.005$. We adopt these parameters throughout.

3.4 Zhang, Fakhouri & Ma (2008)

Zhang et al. (2008b; hereafter Z08) developed three new algorithms (called A, B and C) that all, by construction, satisfy the self-consistency constraint discussed in §2.2.1. And each algorithm can use either the PMF for spherical collapse, based on Eq. (2), or that for ellipsoidal collapse based on Eq. (4). In what follows, we only focus on methods A and B, and refer to them as Z08X[YY], where X is either A or B and YY is either SC (for spherical collapse) or EC (for ellipsoidal collapse).

Overall, the Z08 algorithms are considerably more involved than any of the algorithms discussed above. Here we only sketch the rough idea behind them, and we refer the

interested reader to Zhang et al. (2008b) for details. The Z08 algorithms are similar to that of SK99, in that they allow for more than two progenitors per time-step. The most massive progenitor for a branching point is called the primary progenitor, while all other progenitors are called secondary. The main difference between methods A and B is the mass range over which the primary progenitor is drawn from the PMF: in the case of Method A, this mass range is $[M_0/2, M_0]$. In the case of Method B this mass range is modified to $[\alpha M_0, M_0]$, where α is defined by

$$\int_{\alpha M_0}^{M_0} n_{\text{EPS}}(M_1, z_1 | M_0, z_0) dM_1 = 1. \quad (9)$$

A somewhat unsatisfactory characteristic of the Z08 algorithms is that, if there are multiple secondary progenitors in a given time step, they all have identical masses. In addition, in those cases neither method A nor method B perfectly conserves mass. However, as shown in Z08, despite these shortcomings both methods A and B accurately satisfy the EPS self-consistency constraints, both for the SC and EC cases.

4 PUTTING THE MERGER TREES TO THE TEST

In our comparison of the various merger tree algorithms described above (namely, SK99, C00, P08, Z08A[SC], Z08A[EC], Z08B[SC], and Z08B[EC]), we use the following diagnostics: (i) the progenitor mass function for a tiny time-step, (ii) the mass assembly history of the main progenitor, (iii) the merger rate per descendant halo, and (iv) the unevolved subhalo mass function. These diagnostics are chosen because they have the potential to reveal subtle differences between the various merger-tree algorithms, and because they have been studied using high-resolution cosmological N -body simulations, which provides a benchmark for the comparison. In what follows, we discuss each of these diagnostics in turn.

Throughout what follows we adopt a flat Λ CDM cosmology with $\Omega_{\text{m},0} = 0.25$, $\Omega_{\Lambda,0} = 0.75$, $h = H_0/(100 \text{ km s}^{-1} \text{ Mpc}^{-1}) = 0.73$ and with initial density fluctuations described by a Harrison-Zeldovich power spectrum with normalization $\sigma_8 = 0.9$. We use the transfer function of Eisenstein & Hu (1998) with a baryonic mass density $\Omega_{\text{b},0} = 0.045$. This is exactly the same cosmology as that used for the Millennium simulations (Springel et al. 2005), thus allowing for a direct comparison. We will refer to this cosmology as the ‘Millennium cosmology’.

Unless specifically stated otherwise, we always adopt a time step of $\Delta\omega = 0.002$, independent of which merger tree algorithm we use. This easily meets all the time-step criteria described in the original papers, and we have verified that none of our results are sensitive to this choice for $\Delta\omega$, as long as it doesn’t get significantly larger than ~ 0.01 . Finally, all merger trees are constructed using a mass resolution of $M_{\text{res}} = 10^{-4} M_0$, unless specifically stated otherwise.

4.1 Progenitor Mass Functions

As a first test of the various merger tree algorithms, we check how well they perform in terms of the self-consistency

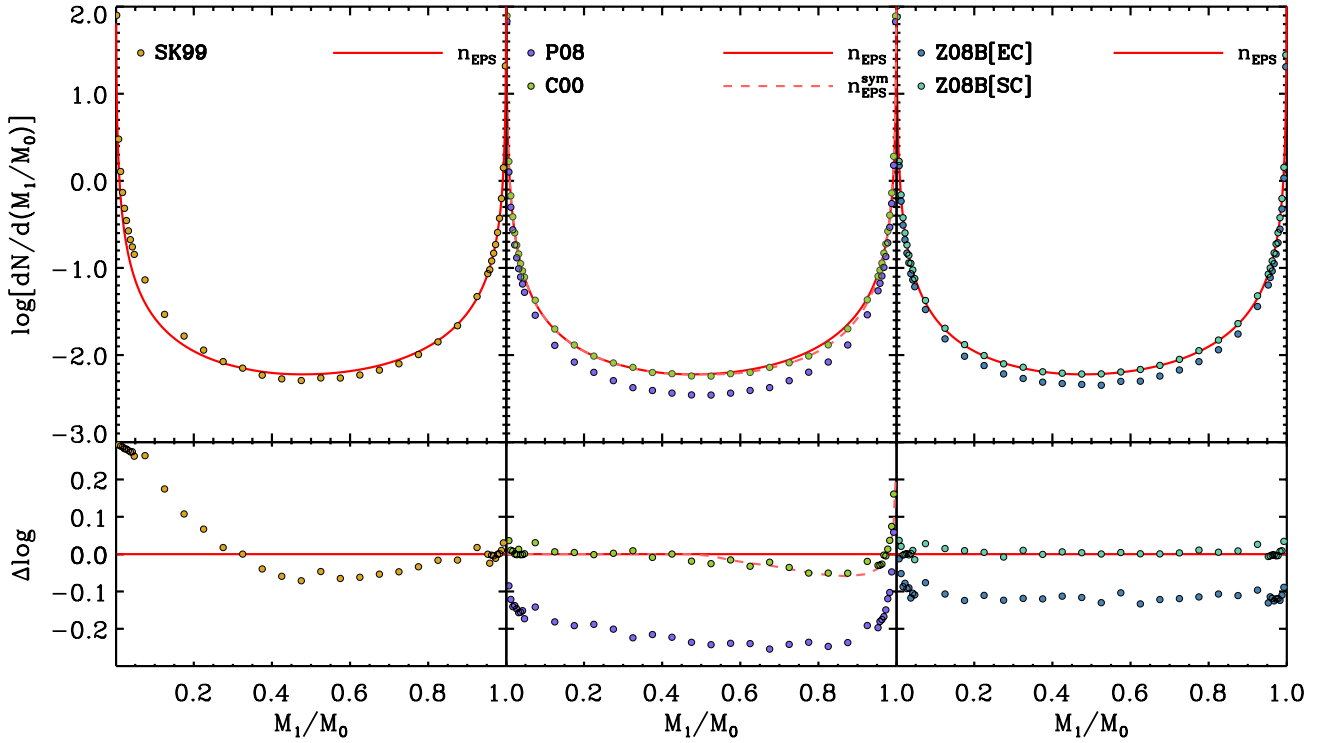


Figure 2. Progenitor mass functions obtained from 10^7 realizations of a single time step with $\Delta\omega = 0.002$, $M_0 = 10^{13} h^{-1}M_\odot$ and $z_0 = 0$ for different merger tree algorithms, as indicated (symbols). The solid line indicates the EPS prediction for spherical collapse (Eq. [2] and [3]), and is shown for comparison. The dashed line in the middle panel is the symmetrized EPS progenitor mass function of Eq. (10), which accurately describes the PMF of the C00 algorithm. Results for the Z08A algorithms are not shown, because they are virtually identical to those of the Z08B algorithm shown in the right-hand panel.

test described in §2.2.1. The symbols in Fig. 2 indicate the progenitor mass functions (PMFs) obtained using 10^7 realizations of a single time step with $\Delta\omega = 0.002$, $M_0 = 10^{13} h^{-1}M_\odot$ and $z_0 = 0$ for the various merger tree algorithms discussed in this paper. The solid line, for comparison, shows the EPS prediction in the case of spherical collapse (Eq. [2] and [3]). Clearly, SK99 does not meet the self-consistency criterion, in that the PMF that results from the algorithm doesn’t match the EPS prediction. This is a consequence of the fact that the SK99 algorithm rejects any progenitor drawn from the EPS PMF that overflows the mass budget.

The C00 algorithm clearly improves upon this, but it still fails to meet the self-consistency criterion (at the few percent level) for $M_p \gtrsim M_0/2$. This is a consequence of the binary assumption inherent to this algorithm. This is evident from the dashed curve in the middle panels of Fig. 2, which shows the symmetrized PMF

$$n_{\text{EPS}}^{\text{sym}}(M_1, z_1|M_0, z_0) \equiv \begin{cases} n_{\text{EPS}}(M_1, z_1|M_0, z_0) & \text{if } M_1/M_0 \leq 0.5 \\ n_{\text{EPS}}(M_0 - M_1, z_1|M_0, z_0) & \text{otherwise} \end{cases} \quad (10)$$

with $n_{\text{EPS}}(M_1, z_1|M_0, z_0)$ given by Eq. (3). Clearly, the binary assumption made in the C00 algorithm results in a PMF that is symmetric with respect to $M_1/M_0 = 0.5$, in disagreement with EPS (see also Neistein & Dekel 2008a).

The P08 algorithm results in a PMF that strongly violates the self-consistency criterion. This is a consequence of the fact that the P08 algorithm sidesteps EPS by using a ‘perturbing’ function that has been calibrated such that the resulting PMF is in agreement with that obtained by Cole et al. (2008) using merger trees extracted from the Millennium simulation. Hence, the blue dots in the middle panel of Fig. 2 are also representative of the PMF in numerical simulations.

The right-hand panel of Fig. 2 shows the results from the Z08B algorithms, both in the case of spherical collapse (green dots) and ellipsoidal collapse (blue dots). Results for the Z08A algorithm are not shown, as they are basically indistinguishable from those of the corresponding Z08B algorithms. Note how the Z08B[SC] algorithm satisfies the EPS self-consistency criterion to high accuracy. Interestingly, the PMF that results from ellipsoidal collapse conditions falls below that for spherical collapse, very similar to the PMF of the P08 method. This immediately suggests that the progenitor mass functions in simulations are more reminiscent of ellipsoidal collapse conditions than of spherical collapse conditions. Note, though, that the PMFs of the P08 and Z08B[EC] methods do differ at the 10 percent level.

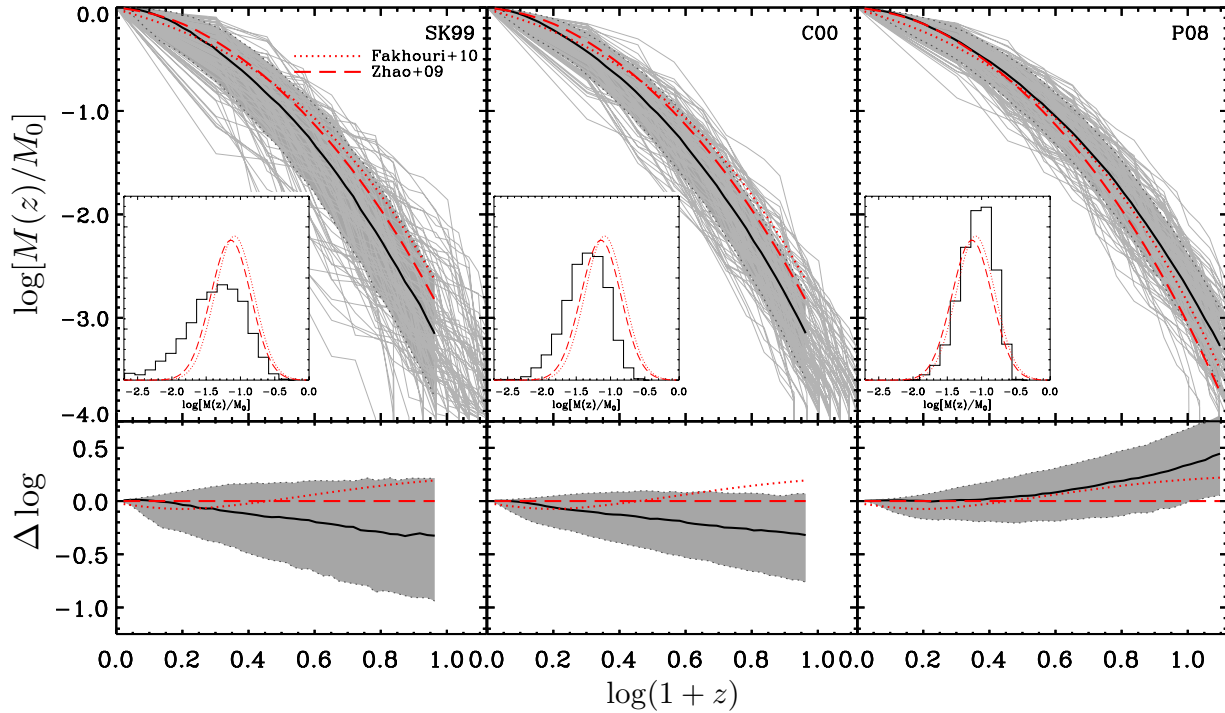


Figure 3. Mass assembly histories (MAHs) for present-day host haloes with $M_0 = 10^{13} h^{-1} M_\odot$ in the Millennium cosmology. The thin, gray lines in the upper panels are 100 random realizations obtained using the merger tree algorithm indicated in the upper-right corner of each panel. The solid black line indicates the median obtained using 2000 MAHs, while the two dotted curves that enclose the shaded region indicate the corresponding 68 percentiles of the distribution in $\log[M(z)/M_0]$ at fixed redshift. Note that we only plot the median and 68 percentiles up to the redshift where the main progenitors of $> 90\%$ of all host haloes in consideration can be traced (i.e., have masses $M > 10^{-4} M_0$), which can vary substantially from one method to the other. For comparison, the red curves are the model predictions of the *median* from Fakhouri et al. (2010, dotted curve) and Zhao et al. (2009, dashed curve), both of which are obtained from numerical simulations. The insets show the distributions of $\log[M(z)/M_0]$ at $z = 3$ (black histograms), as well as two log-normal distributions with the medians taken from the Fakhouri et al. and Zhao et al. models, and with the scatter given by Eq. (11). Finally, the lower panels show the differences in $\log[M(z)/M_0]$ with respect to the Zhao et al. model.

4.2 Mass Assembly Histories

As discussed in §2.1, the mass assembly history (MAH) of a (host) halo is the mass history, $M(z)$, of the halo’s *main* progenitor (also called the zeroth-order progenitor). The MAHs of dark matter haloes have been studied in a large number of papers, using either the EPS formalism (e.g., Lacey & Cole 1993; Eisenstein & Loeb 1996; Nusser & Sheth 1999; van den Bosch 2002) or N -body simulations (e.g., Wechsler et al. 2002; Zhao et al. 2009; McBride et al. 2009; Fakhouri et al. 2010; Yang et al. 2011; Wu et al. 2013). In this section we compare the *median* MAHs obtained using the different merger tree algorithms to fitting functions obtained from N -body simulations.

Zhao et al. (2009) used a set of cosmological N -body simulations (for different cosmologies) to study the mass assembly of dark matter haloes, and generalized from their results a universal model that predicts the *median* MAH for any host halo mass and any cosmology. Yang et al. (2011) subsequently showed that the scatter in $M(z)/M_0$ at fixed z is well described by a log-normal distribution, with median given by the Zhao et al. (2009) model and with a dispersion (in 10-based logarithm) given by

$$\sigma_{\text{MAH}} = 0.12 - 0.15 \log[\mathcal{M}(z)/M_0], \quad (11)$$

where $\mathcal{M}(z)$ is the *median* main-progenitor mass at z . Because of this log-normal form, it is straightforward to compute the *mean* MAH. After all, for a log-normal distribution the *mean* main progenitor mass, $\langle M \rangle$ is related to the median according to

$$\langle M \rangle = \exp \left[\frac{1}{2} \{\ln(10) \sigma_{\text{MAH}}\}^2 \right] \mathcal{M}. \quad (12)$$

Thus, assuming a log-normal distribution, we can convert a *median* MAH into a *mean* MAH, and vice versa.

McBride et al. (2009) used the Millennium simulation (MS) to study the mass assembly history and mass growth rate of dark matter haloes. They provided a fitting formula for the *mean* mass growth rate $\langle \dot{M} \rangle$ as a function of the instantaneous halo mass M and redshift z . In a subsequent paper, Fakhouri et al. (2010) used a combination of the MS I and II simulations to (slightly) revise these results, which resulted in a best-fit, mean mass growth rate

$$\langle \dot{M} \rangle(M, z) = 46.1 M_\odot \text{yr}^{-1} \left[\frac{M(z)}{10^{12} M_\odot} \right]^{1.1} (1 + 1.11 z) \times \sqrt{\Omega_{\text{m},0}(1+z)^3 + \Omega_{\Lambda,0}}. \quad (13)$$

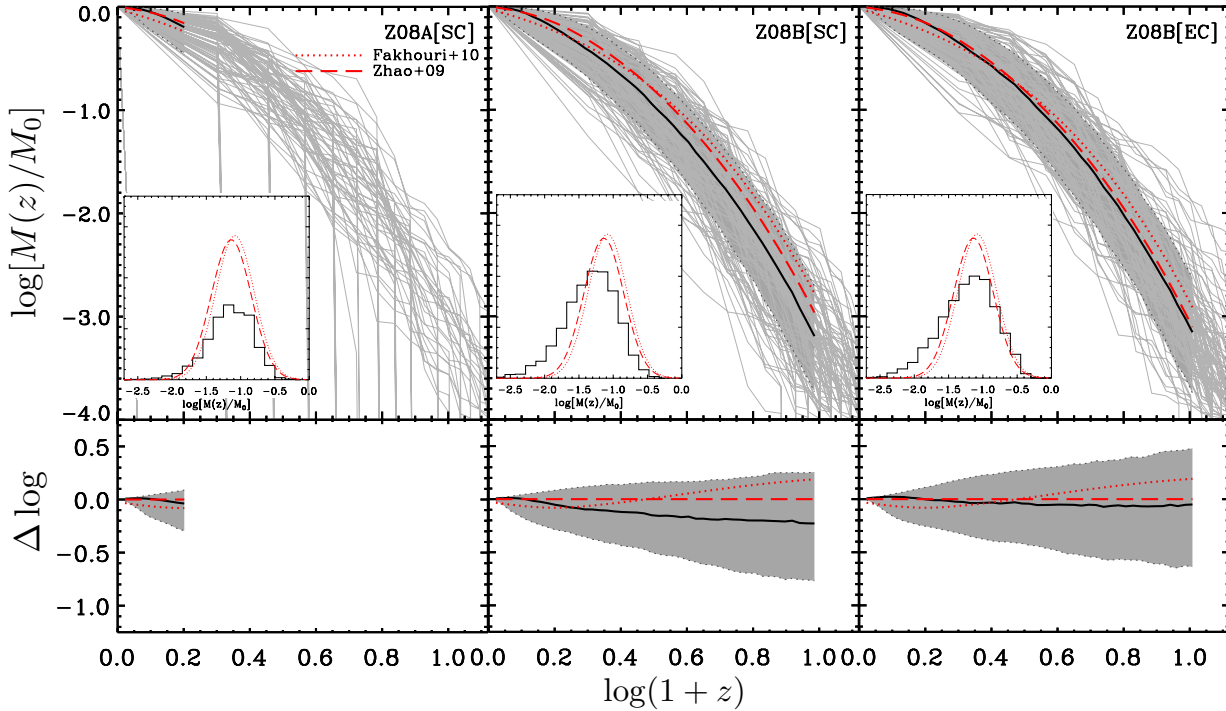


Figure 4. Same as Fig. 3 but for the merger tree algorithms Z08A[SC] (left-hand panels), Z08B[SC] (middle panels) and Z08B[EC] (right-hand panels). Note that the histogram in the inset for Z08A[SC] has a different normalization than the model curves; this reflects the fact that 60% of all MAHs constructed using this algorithm have already dropped below the mass resolution of $10^{-4}M_0$ by $z = 3$.

This can be used to model the *mean* MAH of a halo by simple integration. We caution, though, that Eq. [13] is only valid for the Millennium cosmology.

Finally, Wu et al. (2013) used the Rhapsody cluster re-simulation project to study the MAHs of 96 cluster-size haloes of mass $M_0 = 10^{14.8 \pm 0.05} h^{-1} M_\odot$ at unprecedented resolution (for a halo sample this size). Their *mean* MAH is well fitted by

$$\langle M \rangle(z) = M_0 (1+z)^{-1.46} e^{-0.55z}, \quad (14)$$

where $\gamma = 0.55$.

In what follows, we compare the simulation results of Zhao et al. (2009), Fakhouri et al. (2010) and Wu et al. (2013) to the MAHs obtained using the various merger tree algorithms. Specifically, for a given cosmology and halo mass, we construct 2000 merger trees from which we compute the *median* MAH. When computing the median, it is important to take account of the mass resolution of the merger trees (which we take to be $M_{\text{res}} = 10^{-4}M_0$). Throughout, we follow Zhao et al. (2009) and only perform our statistical analysis of the EPS MAHs up to the redshift where the main progenitors of $> 90\%$ of all host haloes in consideration can be traced (i.e., have $M > 10^{-4}M_0$).

Figs. 3 and 4 plot the MAHs for haloes of $M_0 = 10^{13} h^{-1} M_\odot$ (at $z_0 = 0$) in the Millennium cosmology. The thin, gray curves are the realizations for a random subset of 100 MAHs, while the black solid and dotted curves indicate the median and the 68 percentiles of the distribution of 2000 MAHs. Note that we only plot this median out to

the redshift below which less than 10 percent of the MAHs have dropped below the mass resolution of the merger tree ($10^{-4}M_0$), which can vary substantially from one method to the other. For comparison, the red curves are the model predictions, based on numerical simulations, of Fakhouri et al. (2010) and Zhao et al. (2009), as indicated. In the case of Fakhouri et al. (2010), we integrated their model for the mean mass accretion rate (Eq. [13]) to obtain the *mean* MAH, which we converted to the *median* using Eqs. (11) - (12). The insets in Figs. 3 and 4 show the distributions of $\log[M(z)/M_0]$ at $z = 3$ (black histograms), as well as two log-normal distributions with the medians taken from the Fakhouri et al. and Zhao et al. models, and with the scatter given by Eq. (11). Finally, the lower panels show the differences in $\log[M(z)/M_0]$ with respect to the Zhao et al. model.

The Z08A[SC] method differs from all other methods in that it yields a large fraction of MAHs that drop below the mass resolution at very low redshift. In fact, already at $z \simeq 0.4$, more than 10 percent of the MAHs have dropped below $10^{-4}M_0$. At $z = 3$, this fraction has increased to 40 percent; for all other methods, zero percent of the MAHs have dropped out from the sample by $z = 3$. Similarly large ‘dropout’ fractions are obtained when using method Z08A[EC]. As discussed in Zhang et al. (2008b), this arises due to a subtlety in how method A assigns progenitors, and is the main motivation why the authors considered an alternative; method B. Our results show that this subtlety yields MAHs that are seriously flawed, and we therefore no longer con-

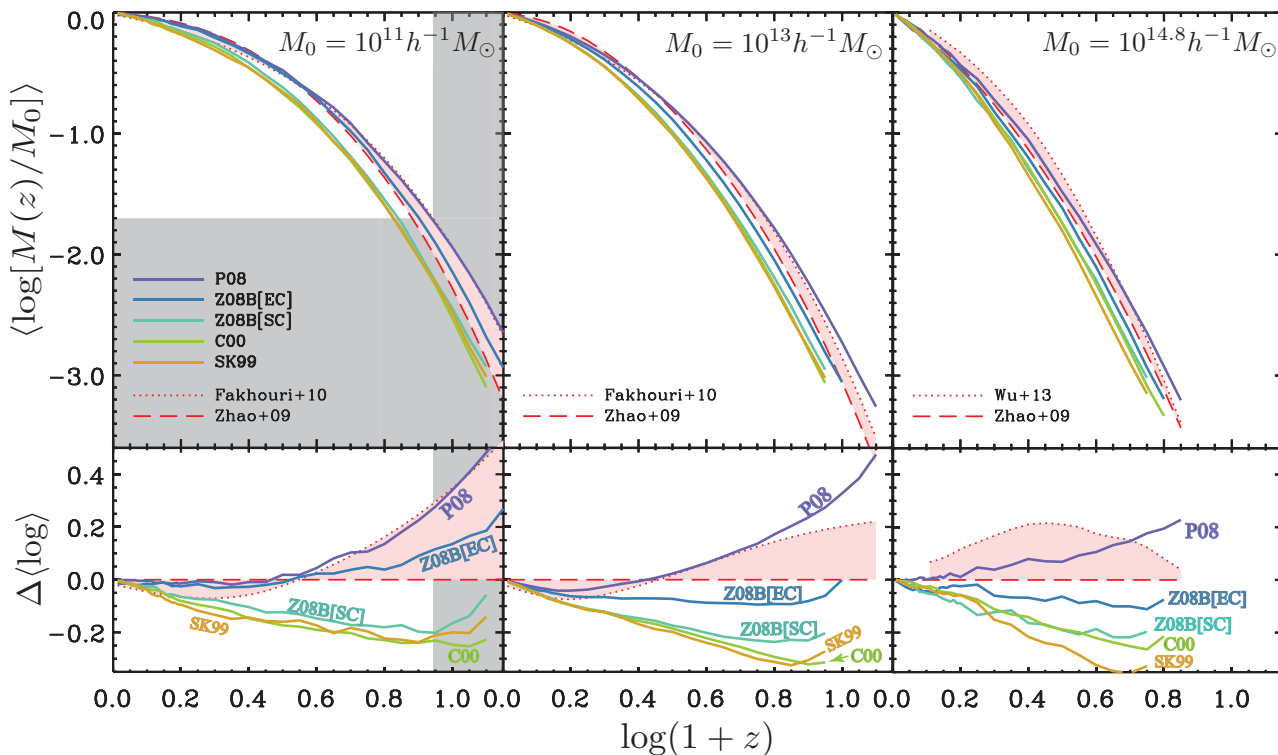


Figure 5. Mean $\log[M(z)/M_0]$ as function of redshift for host haloes at $z = 0$ with masses of $M_0 = 10^{11} h^{-1} M_\odot$ (left-hand panel), $10^{13} h^{-1} M_\odot$ (middle panel), and $10^{14.8} h^{-1} M_\odot$ (right-hand panel). The solid curves are the results obtained using the SK99, C00, P08 and Z08B (both SC and EC) merger tree algorithms, as indicated. In the left and middle panels we have used our fiducial ‘Millennium cosmology’, which allows us to compare the MAHs to the simulation results of Fakhouri et al. (2010; dotted red curve) and Zhao et al. (2009; dashed red curve) model. The gray-shaded region in the left-hand panel roughly marks the mass resolution of the simulations used by Fakhouri et al. and Zhao et al. Hence, the simulation results in this region are largely based on extrapolation, and have to be considered less reliable. In the right-hand panel, in order to facilitate a comparison with the results of Wu et al. (2013; dotted red curve), we have adopted the ‘Rhapsody cosmology’. The lower panels show the residuals with respect to the Zhao et al. model.

sider method Z08A, neither the SC nor the EC version, in what follows.

Comparing the median MAHs obtained using the various EPS algorithms with the simulation results, it is clear that the three spherical-collapse-based algorithms, SK99, C00 and Z08B[SC], share a common feature: they all predict that halo assembly occurs too recent compared to simulations. As already discussed in §2.2.2, this is a well-known problem of SC-based EPS. When comparing the scatter in the MAHs, it is further evident that the SK99 method predicts too much scatter, while the scatter in the C00 MAHs appears to be in good agreement with the simulation results. The Z08B[SC] results are intermediate between those of SK99 and C00. The ellipsoidal collapse based method, Z08B[EC], yields a median MAH in excellent agreement with the simulation results, although the method seems to predict slightly too much scatter. Finally, the MAHs obtained using the P08 method also are in good agreement with simulations, both in terms of the median and in terms of the scatter, although there is some indication that it yields MAHs whose early stages of halo assembly occur too early.

Fig. 5 plots the mean MAHs obtained using SK99, C00, P08 and Z08B (both SC and EC) for host haloes at

$z = 0$ with masses of $M_0 = 10^{11} h^{-1} M_\odot$ (left-hand panel), $10^{13} h^{-1} M_\odot$ (middle panel), and $10^{14.8} h^{-1} M_\odot$ (right-hand panel). Note that contrary to Figs. 3 and 4 we now plot the *mean* of $\log[M(z)/M_0]$, which is identical to the *median* for a log-normal distribution. In the left and middle panels we have used our fiducial ‘Millennium cosmology’, which allows us to compare the EPS-based MAHs to the simulation results of Fakhouri et al. (2010), shown as thick dashed curves. We also show, for the same cosmology, the predictions based on the Zhao et al. (2009) model. The gray-shaded region in the left-hand panel marks the region where the main progenitor mass $M < 2 \times 10^9 h^{-1} M_\odot$. This roughly marks the mass scale below which the simulations used by Zhao et al. (2009) and Fakhouri et al. (2010) can no longer reliably resolve the MAHs. Hence, in the gray region the simulation results are less reliable and largely based on extrapolation. Ignoring this region, the Fakhouri et al. and Zhao et al. models agree roughly at the 0.1-0.2 dex level. In the right-hand panel, in order to facilitate a comparison with the results of Wu et al. (2013), we adopt the Rhapsody cosmology (which has lower σ_8 than the Millennium cosmology, and a slightly different Hubble parameter). Again, the agreement between

different simulation results, here between Wu et al. and Zhao et al., is (only) at the level of 0.1-0.2 dex.

A comparison with the MAHs obtained using the various merger tree algorithms shows once again that the three SC-based algorithms (SK99, C00 and Z08B[SC]) yield MAHs that systematically fall below the simulation results. In fact, it is interesting how similar the average MAHs obtained with these very different methods are. The P08 and Z08B[EC] algorithms yield MAHs that are in reasonable agreement with the simulation results; whereas P08 seems to overpredict $M(z)/M_0$ at early times, Z08B[EC] seems to slightly underpredict $M(z)/M_0$ for the most massive haloes.

To summarize, EPS merger trees based on spherical collapse consistently yields mass assembly histories in which haloes assemble too late compared to simulations. In terms of halo substructure, this implies that the SK99, C00 and Z08[SC] algorithms will all underpredict the accretion redshifts of subhaloes, and are therefore not well suited to build analytical models for dark matter substructure or to model satellite galaxies. Both the P08 and Z08B[EC] algorithms fare much better in that respect. They both yield MAHs in reasonable agreement with numerical simulations, both in terms of their median as well as the scatter. The median MAHs predicted by these two methods are in excellent agreement with each other, and with the simulation results at low redshifts ($z \lesssim 2$), but start to diverge at larger redshifts. At $z = 7$ they typically differ at the 0.3 dex level. Unfortunately, because of the ~ 0.2 dex discrepancy among the different simulation results, we cannot significantly prefer one of these two methods over the other.

4.3 Merger Rate per Descendent Halo

The next diagnostic to consider for our EPS merger tree algorithms is the merger rate per descendant halo, $(1/N)d\mathcal{N}_{\text{merger}}/d\omega dx$, which characterizes the rate at which the population of haloes of mass $M = M_1 + M_2$ is created by mergers between progenitors with a mass ratio $x \equiv M_1/M_2$. Here the notation is such that $M_i \geq M_{i+1}$, which implies that $x \geq 1$. The quantity $d\mathcal{N}_{\text{merger}}(M, z, x)/d\omega dx$ is the number of merger events of mass ratio $x \pm dx/2$ that result in descendent haloes of mass $M \pm dM/2$ per unit time interval $d\omega$ at redshift z , and N is the number of descendent haloes of mass $M \pm dM/2$.

Both Fakhouri et al. (2010; hereafter F10) and Genel et al. (2010; hereafter G10) measured this merger rate per descendant halo from the Millennium simulations. A problem is that the time steps between successive outputs of the Millennium simulations are relatively large, and a descendant halo often has more than two progenitor haloes at the previous time step. Both F10 and G10 deal with this complication in the same way: whenever a multiple merger event, consisting of N_p progenitors, occurs they interpret this as a series of $N_p - 1$ binary mergers between M_1 and M_i where $i = 2, 3, \dots, N_p$. Although this is not necessarily a proper description of the true merger history during this time step, this procedure can be repeated using the EPS formalism, thus allowing for a fair comparison.

Using a combination of the Millennium I and Millennium II simulations, F10 and G10 found that the merger rate per descendant halo, for the Millennium cosmology, is well described by;

$$\frac{1}{N} \frac{d\mathcal{N}_{\text{merger}}}{d\omega dx}(M, z, x) = f(z) \left[\frac{M(z)}{10^{12} M_\odot} \right]^{a_1} x^{a_2} e^{a_3 x^{a_4}}, \quad (15)$$

where

$$f(z) = \begin{cases} 0.065 & \text{(G10)} \\ 0.010 \frac{dz}{dz} (1+z)^{a_5} & \text{(F10)} \end{cases} \quad (16)$$

and the best-fit parameters are $(a_1, a_2, a_3, a_4) = (0.15, -0.3, 1.58, -0.5)$ and $(a_1, a_2, a_3, a_4, a_5) = (0.133, -0.005, 3.38, -0.263, 0.0993)$ for the G10 and F10 results, respectively. Note that the fitting equation of G10 is only valid over the range $0.5 \lesssim z \lesssim 5$. The dashed and dotted curves in Fig. 6 show the merger rates per descendant halo according to these F10 and G10 fitting formula, as indicated. They are in reasonable, mutual agreement for $x \lesssim 10$, but diverge quite strongly for larger values of the merger mass ratio. In particular, F10 predicts roughly two times as many minor mergers with $x = 1000$ as G10. This discrepancy mainly arises from the subtle differences in how these authors extract halo merger trees from their simulation outputs (see F10 and G10 for details). As with the MAHs, we are therefore forced to conclude that different authors obtain halo merger rates that differ substantially, even when they base their results on the same simulation. In what follows, we will simply treat this discrepancy between the F10 and G10 results as a rough indicator of the uncertainty on $(1/N)d\mathcal{N}_{\text{merger}}/d\omega dx$ in simulations.

Using EPS merger trees, it is straightforward to compute the merger rate per descendant halo. For a given host halo mass, M_0 , at a given redshift, z_0 , we construct $N = 10,000$ realizations of the population of progenitor haloes a time $\Delta\omega = 0.002$ earlier. These are used to compute the merger rate per descendant halo, strictly following the procedure used by F10 and G10 to treat multiple mergers. Fig. 6 compares the results obtained using our five remaining merger tree algorithms to the fitting functions of F10 and G10. All merger rates in this figure are for a redshift $z_0 = 1$, while different panels correspond to different host halo masses, as indicated. We have verified that the results look almost indistinguishable at any other redshift in the range $0.5 \leq z_0 \leq 5$. We have also verified that the results are not sensitive to the temporal resolution, as we vary $\Delta\omega$ between 0.001 and 0.1, the merger rates at $z_0 = 1$ change by no more than 10%.

Upon inspection a number of trends are apparent. First of all, the merger rates obtained with the C00 and Z08B[SC] algorithms are virtually indistinguishable. Both over-predict the rate of major mergers (mergers with $x \lesssim 3$) by a factor of about two with respect to the numerical simulation results of F10 and G10. This discrepancy becomes smaller for larger x , at least when compared to the F10 fitting function. Interestingly, compared to the G10 fitting function the C00 and Z08B[SC] merger rates follow almost exactly the same x -dependence, but with a normalization that is a factor ~ 2 too high. A similar trend was noticed by G10. The third spherical collapse algorithm, SK99, dramatically over-predicts the merger rates of dark matter haloes compared to both G10 and F10, for all host halo masses (and at all redshifts). The discrepancy is most pronounced for mergers with a mass ratio $x \sim 20$, for which SK99 predicts a rate that is a factor three to four too high. This failure of the

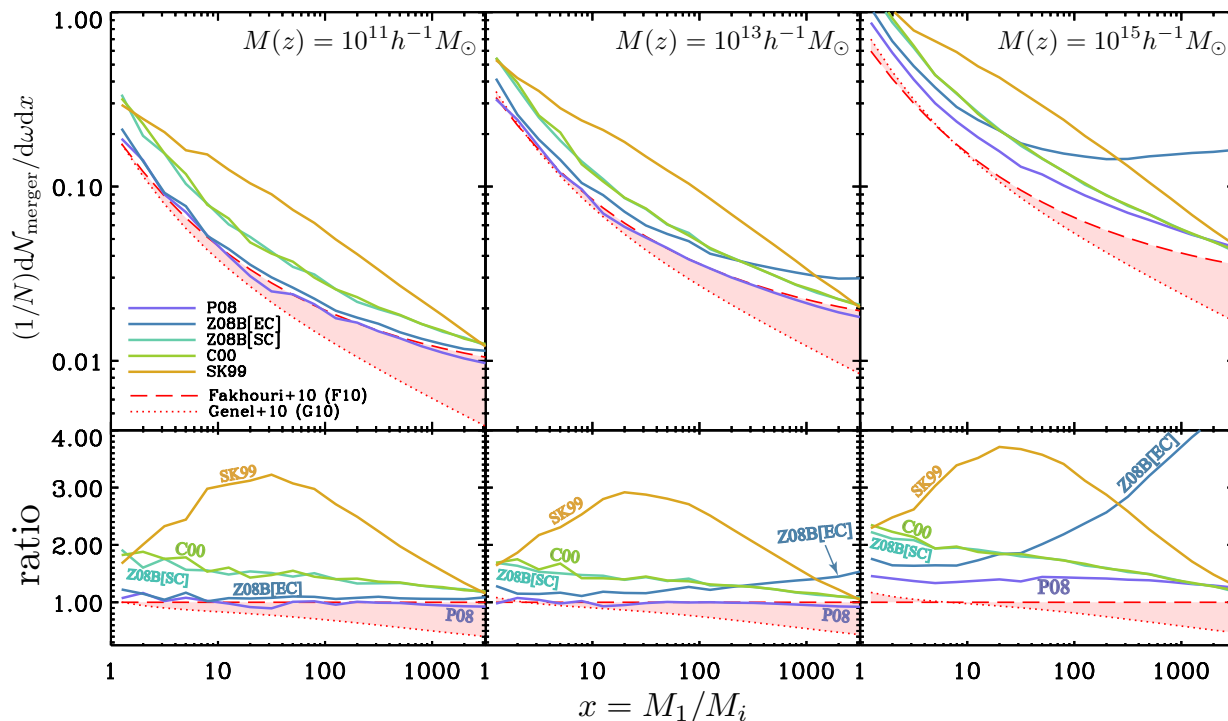


Figure 6. Upper panels plot the merger rate per descendant halo, $dN_{\text{merger}}/d\omega dx$, as a function of the merger mass ratio $x \equiv M_1/M_i$ ($i = 2, 3, \dots$, see text for details). Results are shown for descendant haloes at $z = 1$ with masses of $M(z) = 10^{11} h^{-1} M_{\odot}$ (left-hand panels), $10^{13} h^{-1} M_{\odot}$ (middle panels) and $10^{15} h^{-1} M_{\odot}$ (right-hand panels). The solid curves are the results obtained using the SK99, C00, P08 and Z08B (both SC and EC) merger tree algorithms, as indicated, using 10,000 realizations as described in the text. The dashed and dotted red curves are the N -body results obtained using the Millennium simulation by Fakhouri et al. (2010) and Genel et al. (2010), respectively. The lower panels show the residuals with respect to the Fakhouri et al. results.

SK99 algorithm is a direct manifestation of its failure to satisfy the EPS self-consistency constraint.

The ellipsoidal-collapse algorithm Z08B[EC] yields an excellent match to the F10 merger rates for haloes with $M_0 = 10^{11} h^{-1} M_{\odot}$. However, there is a clear trend that the Z08B[EC] algorithm starts to overpredicts the merger rates (compared to F10 and G10) for more massive haloes. This problem is more pronounced for mergers with a larger mass ratio. For cluster-size host haloes with $M_0 = 10^{15} h^{-1} M_{\odot}$, and compared to F10, the Z08B[EC] algorithm overpredicts the major merger rate by a factor 1.7 and that of minor mergers with mass ratio $x = 1000$ by a factor 3.7. We believe that this problem arises from the method used to assign halo masses to the secondary progenitors, which are all assigned the same mass (see §3.4 and Zhang et al. 2008 for details). Finally, the P08 algorithm yields merger rates that are in excellent agreement with the F10 results. The only exception seems to be for cluster-size haloes with $M_0 = 10^{15} h^{-1} M_{\odot}$, where the P08 merger rates are a factor ~ 1.3 too high compared to the F10 fitting function.

To summarize, EPS merger tree algorithms that are based on spherical collapse overpredict the rate of major mergers by about a factor of two. Ellipsoidal collapse seems able to alleviate this tension. However, the Z08B[EC] implementation of ellipsoidal collapse has a problem in that it vastly overpredicts the number of minor mergers for mas-

sive host haloes. Overall, the P08 algorithm yields merger rates in significantly better agreement with the simulation results than any of the other merger tree algorithms considered here. It still overpredicts the merger rates for cluster size host haloes by about 30 percent, but we emphasize that the disparity in merger rates obtained by different authors from the same simulation are of a similar magnitude.

4.4 The Unevolved Subhalo Mass Function

The final diagnostic that we consider for testing the various EPS merger tree algorithms is the unevolved subhalo mass function (hereafter USMF), $dN/d \ln(m/M_0)$, where m is the mass of the subhalo at accretion, and M_0 is the present-day host halo mass.

Using EPS merger trees, van den Bosch, Tormen & Giocoli (2005) noticed that the USMF of first-order subhaloes (i.e., only counting those subhaloes that accrete directly onto the main progenitor) is universal, in that it doesn't reveal any significant dependence on either host mass, redshift, or cosmology. This was later confirmed by Giocoli et al. (2008; hereafter G08) and Li & Mo (2009; hereafter LM09) using numerical simulations. Note, though, that this universality is only approximate. It is adequate for host haloes with masses in the range $10^{10} h^{-1} M_{\odot} \lesssim M_0 \lesssim 10^{15} h^{-1} M_{\odot}$ in a Λ CDM cosmology, but does not necessarily hold for more extreme

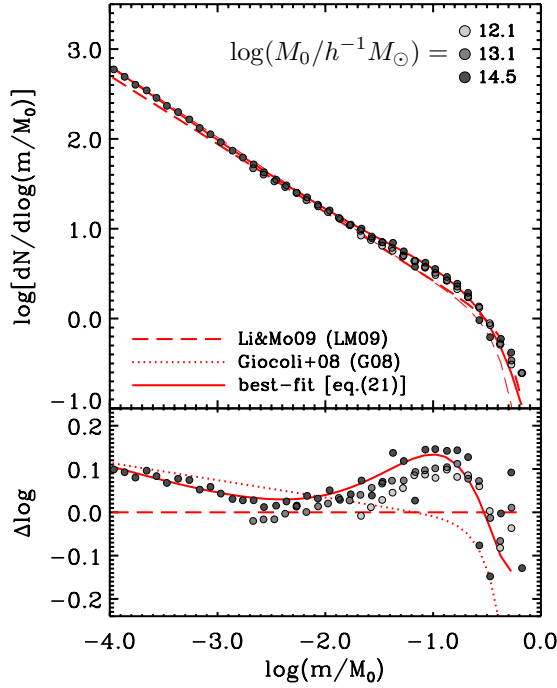


Figure 7. The unevolved subhalo mass function of first order subhaloes (USMF[1]). Symbols are the results obtained by Li & Mo (2009; LM09) using the Millennium simulation, for three different bins in host halo mass, as indicated. The dotted and dashed curves are the fitting functions obtained by Giocoli et al. (2008; G08) and LM09, respectively, while the solid line is the best-fit fitting function of the form given by Eq. (21). The lower panel shows the residuals with respect to the LM09 fitting function. Note that our new fitting function, which has more freedom, better describes the ‘shoulder’ around $\log(m/M_0) \simeq -1$.

halo masses and/or cosmologies. Indeed, using simulations for cosmologies with scale-free power spectra, $P(k) \propto k^n$, Yang et al. (2011) has shown that the USMF depends significantly on the value of the spectral index n . The apparent universality noticed by van den Bosch et al. (2005), G08 and LM09 arises because the effective spectral index of the Λ CDM power spectrum only varies slightly over the mass range $10^{10} h^{-1}M_\odot \leq M_0 \leq 10^{15} h^{-1}M_\odot$.

Using the universality of the USMF of first-order subhaloes, it is straightforward to compute the USMF of n^{th} -order subhaloes, which is defined as the mass function of n^{th} order subhaloes at their moment of accretion (i.e., when they transit from being host haloes to being subhaloes). After all, since subhaloes can themselves be considered as host haloes at the time of accretion, their sub-haloes, which are of second-order, are also expected to obey the universal USMF. As emphasized in LM09, this implies that

$$n_{\text{un},i}(m|M_0) = \int_0^{M_0} n_{\text{un},1}(m|m_a) n_{\text{un},i-1}(m_a|M_0) dm_a, \quad (17)$$

(for $i = 2, 3, \dots$). Here

$$n_{\text{un},i}(m|M_0) \equiv \frac{dN}{dm} = \frac{1}{m} \frac{dN}{d \ln(m/M_0)}, \quad (18)$$

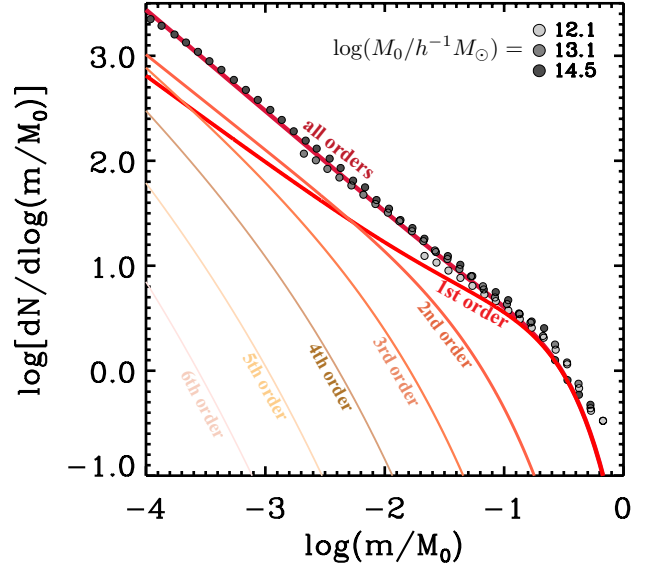


Figure 8. The unevolved subhalo mass functions (USMF) for different order subhaloes, as indicated. The first-order USMF is characterized by the fitting function of Eq. (21) with the best-fit parameters given in the text, while the higher-order USMFs have been computed from this first-order USMF using Eq. (17). The data points are the simulation results for *all* order subhaloes obtained by LM09 using the Millennium simulation, for three different bins in host halo mass, as indicated. The solid line labeled ‘all orders’ is the corresponding analytical prediction, which has been computed by summing the USMFs for order one to four (the contribution of higher order USMFs is negligible). The fact that this prediction is an excellent match to the data supports the notion that the first-order USMF is universal.

is the i^{th} -order unevolved subhalo mass function, for which we will use the shorthand $\text{USMF}[i]$ in what follows.

Using the high resolution GIF simulations, G08 found that the $\text{USMF}[1]$ is well fit by

$$\frac{dN}{d \ln(m/M_0)} = \gamma \left(\frac{m}{M_0} \right)^\alpha \exp \left[-\beta \left(\frac{m}{M_0} \right)^\zeta \right], \quad (19)$$

with best-fit parameters $(\gamma, \alpha, \beta, \zeta) = (0.18, -0.80, 12.27, 3.00)$. Note that this implies a total normalization

$$\begin{aligned} F_{\text{norm}} &\equiv \frac{1}{M_0} \int_0^{M_0} m \frac{dN}{dm} dm \\ &= \int_0^1 \frac{dN}{d \ln(m/M_0)} d(m/M_0) \simeq 0.735. \end{aligned} \quad (20)$$

The fact that F_{norm} is substantially smaller than unity implies that dark matter haloes accrete a significant fraction of their mass ‘smoothly’, either in the form of matter not locked up in any halo or in the form of haloes with masses below the resolution limit of the simulation[‡].

LM09 used the Millennium simulations and found slightly different best-fit parameters, given by $(\gamma, \alpha, \beta, \zeta) = (0.2, -0.76, 6.00, 3.20)$, for which $F_{\text{norm}} \simeq 0.701$. The open

[‡] Note, though, that the values for F_{norm} quoted here are based on extrapolating fitting functions for the $\text{USMF}[1]$ to subhalo masses well below the mass resolution of the simulations.

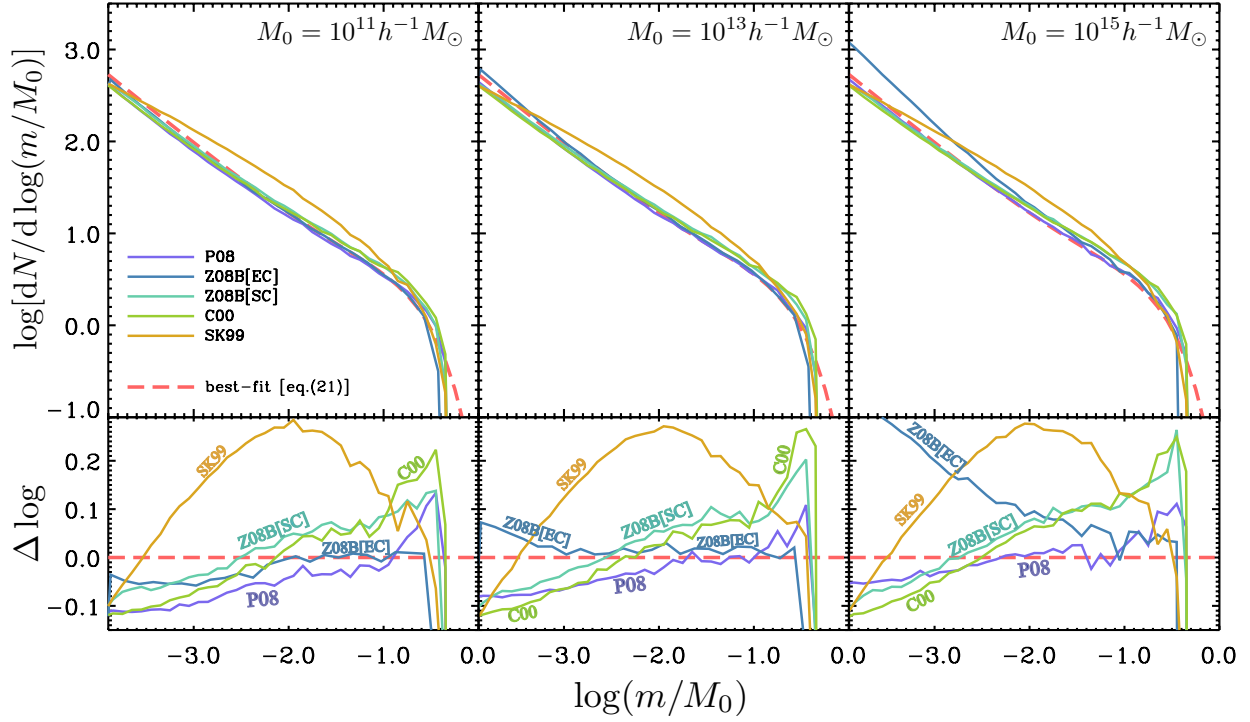


Figure 9. The unevolved subhalo mass function of first order subhaloes (USMF[1]) for host haloes (at $z = 0$) with mass $M_0 = 10^{11} h^{-1} M_\odot$ (left-hand panels), $10^{13} h^{-1} M_\odot$ (middle panels) and $10^{15} h^{-1} M_\odot$ (right-hand panels). The solid curves are the results obtained using the SK99, C00, P08 and Z08B (both SC and EC) merger tree algorithms, as indicated. For comparison, the red, dashed line indicates the best-fit representation of the simulation results given by Eq. (21) with the best-fit parameters given in the text (cf. red, solid curve in Fig. 7). The lower panels show the residuals with respect to these simulation results.

circles in Fig. 7 are the actual data used by LM09 in their fitting procedure, for three different bins in host halo mass, as indicated. The dotted and dashed curves are the best-fit functions (19) obtained by G08 and LM09, respectively. As is apparent from the lower panel, showing the residuals, neither is a good fit to the actual data. In particular, the LM09 data reveals a clear ‘shoulder’ around the mass scale where the exponential cut-off kicks in. Since this feature is not captured by the fitting function of the form (19), we adopt an alternative fitting function for the USMF, which simply is a linear combination of two components of the form (19), but with a common exponential-decay part:

$$\frac{dN}{d \ln(m/M_0)} = \left[\gamma_1 \left(\frac{m}{M_0} \right)^{\alpha_1} + \gamma_2 \left(\frac{m}{M_0} \right)^{\alpha_2} \right] \times \exp \left[-\beta \left(\frac{m}{M_0} \right)^\zeta \right]. \quad (21)$$

Using the simulation results of LM09, we obtain the following best-fit parameters: $(\gamma_1, \alpha_1, \gamma_2, \alpha_2, \beta, \zeta) = (0.13, -0.83, 1.33, -0.02, 5.67, 1.19)$, which is shown as the solid line in Fig. 7. Note that this USMF[1] has a normalization $F_{\text{norm}} = 0.8625$, significantly larger than for the G08 and LM09 fitting functions, which reflects the ‘extra’ mass under the shoulder. In what follows we will use this new fitting function for the USMF[1] as the benchmark for our various EPS merger tree algorithms. As a cautionary remark, we point out that the simulations used by both G08

and LM09 have a mass resolution of $\sim 2 \times 10^{10} h^{-1} M_\odot$, and our fitting function therefore has to be considered an extrapolation for any $m \lesssim 2 \times 10^{10} h^{-1} M_\odot$.

We have used our best-fit fitting function for the USMF[1] to compute the USMF for subhaloes of higher-order. The results are shown in Fig. 8, where different curves correspond to USMFs for different order, as indicated. Note how USMF[2] is higher than USMF[1] for $m/M_0 \lesssim 3 \times 10^{-2}$, and dominates the total USMF, defined as the sum of USMF[i] for all i , over the entire range $-4 \leq m/M_0 \lesssim -2$. The contribution to the total USMF due to subhaloes of order 5 or higher is negligible for all $m/M_0 > 10^{-4}$. The data points in Fig. 8 are the simulation results for *all* order subhaloes obtained by LM09 using the Millennium simulation. Note that our prediction for this USMF[all], which we compute by summing USMF[i] for $i = 1$ to 4, is in excellent agreement with these data[§].

4.4.1 The Unevolved Subhalo Mass Function of First-Order

Fig. 9 compares the USMF[1] obtained using the various EPS merger tree algorithms to our best-fit representation of the simulation results (dashed line). Results are shown

[§] As shown in LM09, this USMF[all] is accurately fit by Eq.(19) with $(\gamma, \alpha, \beta, \zeta) = (0.22, -0.91, 6.00, 3.00)$.

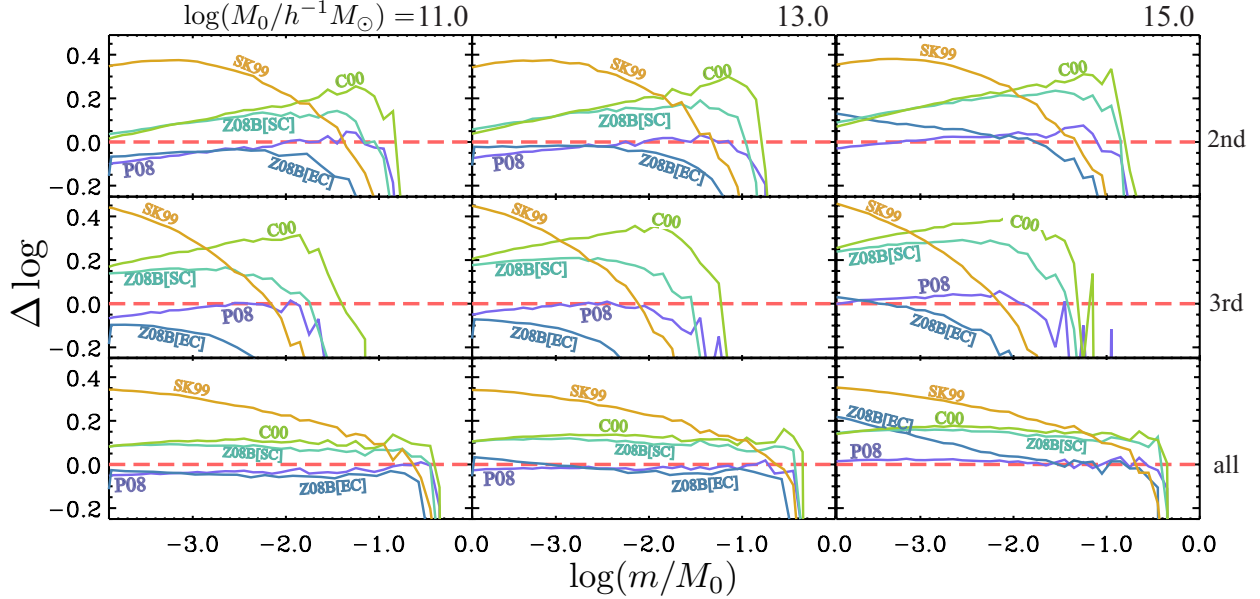


Figure 10. Same as the lower panels of Fig. 9 but for second-order subhaloes (upper row of panels), third-order subhaloes (middle row of panels) and for all orders of subhaloes (lower row of panels). The latter is computed by summing the USMFs of orders one to four. See text for a detailed discussion.

for host haloes at $z = 0$ with $M_0 = 10^{11} h^{-1} M_\odot$ (left-hand panel), $10^{13} h^{-1} M_\odot$ (middle panel) and $10^{15} h^{-1} M_\odot$ (right-hand panel). Overall the results are very similar to those for the merger rate per descendant halo (cf. Fig. 6). Of all the merger-tree algorithms considered, SK99 clearly yields the most discrepant results, overpredicting the USMF[1] by almost 0.3 dex for subhaloes with $m \sim M_0/100$. The C00 and Z08B[SC] algorithms yield results that are very similar, and in significantly better agreement with the simulation results. However, they both underpredict the USMF[1] for low masses (by about 0.1 dex for $\log(m/M_0) = -4$), and overpredict it for the most massive subhaloes (by about 0.2 dex for $\log(m/M_0) = -0.5$). This means that using either of these algorithms will overpredict the abundance of massive subhaloes (satellite galaxies) by about 50 percent. The Z08B[EC] algorithm yields an USMF[1] that is in excellent agreement with the simulation results for a host halo with $M_0 = 10^{11} h^{-1} M_\odot$. However, for more massive host haloes it starts to overpredict the USMF[1] at the low mass end. This becomes fairly dramatic for $M_0 = 10^{15} h^{-1} M_\odot$, where the discrepancy exceeds 0.2 dex for $m < M_0/1000$. Finally, as for the merger rates per descendant halo, the overall best results are clearly obtained with the P08 algorithm, although it still reveals deviations from our benchmark curve of $\lesssim 0.1$ dex. In particular, it slightly over(under)-predicts the number of massive (low mass) subhaloes compared to the results obtained from numerical simulations

4.4.2 The Unevolved Subhalo Mass Function of Higher Order

The upper and middle rows of panels in Fig. 10 show the residuals of USMF[2] and USMF[3] obtained with the various merger tree algorithms compared to the analytical predictions based on Eq. (17). A few trends are apparent. First of all, the USMFs obtained with SK99, C00 and Z08B[SC]

all become progressively worse for higher order subhaloes, overpredicting the USMF by large amounts at the low mass end. The USMFs obtained using the Z08B[EC] method also become progressively worse for higher order, but in the sense that it starts to underpredict the USMF at the massive end. The higher order USMFs obtained using the P08 method, however, become progressively better with increasing order. The lower panels of Fig. 10 show similar residuals but for the USMF of *all* subhaloes, here defined as the sum of all USMF[i] for $i = 1, 2, \dots, 4$ (as discussed above, the contribution from higher order USMFs is negligible for $m/M_0 \geq 10^{-4}$). The P08 predictions are in excellent agreement with the analytical prediction, which in turn is in excellent agreement with the simulation results (cf. Fig. 8). The predictions based on the Z08B[EC] method performs almost equally well for $M_0 < 10^{13} h^{-1} M_\odot$, but over-predicts the abundance of small subhaloes ($m \lesssim 10^{-2} M_0$) for more massive host haloes. The three SC-based algorithms, SK99, C00 and Z08B[SC] all overpredict the USMF[all] by significant amounts. In the case of C00 and Z08B[SC], the offset is roughly independent of subhalo mass, such that they at least predict the correct power-law slope for the USMF[all]. The SK99 algorithm, on the other hand, predicts a power-law slope that is clearly too steep.

5 CONCLUSION AND DISCUSSION

In this paper we have compared and tested a number of different algorithms for constructing halo merger trees. The diagnostics that we have used are the progenitor mass functions (PMF), the mass assembly histories (MAHs), the merger rates per descendant halo, and the unevolved subhalo mass function (USMF).

Of all the algorithms tested, the one that fares worst is that of SK99. The main reason is the strong violation of the

self-consistency constraint (i.e., the progenitor masses drawn fail to sample the actual PMF), which arises from the fact that the SK99 algorithm discards progenitor masses drawn from the PMF that overflow the mass budget (see §3.1 for details). In general, the SK99 algorithm yields (i) haloes that assemble too late, (ii) too much scatter in halo MAHs, (iii) merger rates that are too high by factors of two to three, and (iv) unevolved subhalo mass functions that are much too high, especially for subhaloes with a mass at accretion $m \sim M_0/100$. The latter explains why van den Bosch et al. (2005) inferred an average subhalo mass loss rate that is too high, as previously pointed out by Giocoli et al. (2008). It also implies that other models for dark matter substructure that also used the SK99 algorithm (Taylor & Babul 2004, 2005; Zentner & Bullock 2003; Zentner et al. 2005; Purcell & Zentner 2012), are likely to suffer from similar systematic errors.

The various methods introduced by Z08 have the advantage that, by construction, they accurately satisfy the self-consistency constraint. This is true for both the spherical and ellipsoidal collapse based methods. We have tested and compared both methods A and B, and both for SC and EC. Method A, however, is flawed in that it yields MAHs that are unrealistic (see the left-hand panel of Fig. 4), which is why we haven't considered this method for any of the other diagnostics. Method B, however, fares much better. The SC implementation yields MAHs that assemble too late compared to simulations, and overpredicts the major-merger rate by a factor of two. These are generic problems for SC-based EPS, and are therefore shared by the SK99 and C00 algorithms. The Z08B[SC] algorithm also overpredicts the USMF at the massive end, by about 50 percent. This problem is present for each order of the USMF. At the low mass end (i.e., for $m/M_0 \sim 10^{-4}$), the Z08B[SC] method underpredicts the abundance of first-order subhaloes, but overpredicts that of higher-order subhaloes.

The ellipsoidal collapse implementation of method B, Z08B[EC], solves most of these problems. In particular, it yields MAHs, merger rates and USMFs that are in much better agreement with simulation results. However, the Z08B[EC] algorithm dramatically overpredicts the minor merger rate for massive (cluster-size) host haloes. This in turn results in USMFs for such host haloes that are much too high at the low mass end. We believe that this failure of the Z08B[EC] algorithm has its origin in the fact that it assigns all progenitors of a descendant halo, other than the most massive one, the same mass.

The binary merger method developed by C00 yields halo merger trees that are extremely similar to those constructed with the Z08B[SC] algorithm. In particular, it yields MAHs that assemble too late, overpredicts the major-merger rate by a factor of two, and overpredicts the USMF of first-order subhaloes at the massive end. The small (largely insignificant) differences with respect to the Z08B[SC] algorithm mainly come from the fact that the C00 method violates the self-consistency constraint, but only for progenitors with a mass more than half the descendant mass, and only by a few percent.

Of all the algorithms tested, the one that yields results in closest agreement with the simulations is the P08 algorithm. It slightly overpredicts the merger rates for massive descendant haloes, by about 20 percent, and underpredicts

the USMF for first-order subhaloes at the low mass end, by about 15 percent, but given the uncertainties in the actual simulation results, these discrepancies are barely significant. The fact that the P08 method yields the best results should not come entirely as a surprise. After all, P08 draws its progenitor masses from a PMF that has been modified with respect to the EPS prediction to match the simulation results presented in Cole et al. (2008). Hence, one ought to expect that the P08 algorithm yields results in better overall agreement with simulations. We emphasize, though, that even if a method is tuned to reproduce the PMF of simulations, there is no guarantee that it reproduces any of the other diagnostics. This requires a merger tree algorithm that successfully partitions the descendant mass over progenitors, which is a non-trivial task (as discussed in §2.2.1).

An important (but unavoidable) caveat of the work presented in this paper is that the benchmarks that we have used to test the various merger tree algorithms are all based on numerical simulations. As discussed in §2, and as highlighted in this paper, simulation results carry significant uncertainties that mainly arise from issues related to identifying haloes and tracking them across different simulation outputs. The most problematic aspect is how to properly link (sub)haloes between different snapshots in a manner that properly accounts for the fact that some sub-haloes are on orbits that take them outside the host halo's virial radius. As we have shown, the discrepancies in average halo mass assembly histories or merger rates per descendant halo obtained from simulations by different authors can easily exceed 50 percent, even when they are based on the same simulation. Clearly, this situation has to improve if the goal is to build (semi)-analytical models that are accurate to this level or better. At this point in time, though, taking these uncertainties into account, we conclude that the accuracy of the P08 merger tree algorithm is not significantly worse than that of the simulations themselves.

As a final remark, we point out that there are several other EPS or EPS-based algorithms that can be used to construct merger trees (e.g., Kauffman & White 1993; Neistein & Dekel 2008a,b; Moreno et al. 2008; method C of Zhang et al. 2008). Our choice not to include those methods in this study is simply to keep the project manageable and to prevent the paper from becoming overly dense. However, we believe it would be useful to perform similar tests for these alternative methods as well, and we encourage the community to do so.

ACKNOWLEDGMENTS

We thank the organizers of the program ‘‘First Galaxies and Faint Dwarfs: Clues to the Small Scale Structure of Cold Dark Matter’’ held at the Kavli Institute for Theoretical Physics (KITP) in Santa Barbara for creating a stimulating, interactive environment that started the research presented in this paper, and the KITP staff for all their help and hospitality. We also wish to thank Andrew Wetzel and Andrew Zentner for helpful discussions. This research was supported in part by the National Science Foundation under Grant No. PHY11-25915.

REFERENCES

- Behroozi P.S., Wechsler R.H., Wu H.Y., Busha M.T., Klypin A.A., Primack J.R., 2013, *ApJ*, 763, 18
- Benson A.J., Baugh C.M., Cole S., Frenk C.S., Lacey C.G., 2000, *MNRAS*, 316, 107
- Bond J.R., Cole S., Efstathiou G., Kaiser N., 1991, *ApJ*, 379, 440
- Bower R.G., 1991, *MNRAS*, 248, 332
- Cole S., 1991, *ApJ*, 367, 45
- Cole S., Aragon-Salamanca A., Frenk C.S., Navarro J.F., Zepf S.E., 1994, *MNRAS*, 271, 781
- Cole S., Lacey C.G., Baugh C.M., Frenk C.S., 2000, *MNRAS*, 319, 168 [C00]
- Cole S., Helly J., Frenk C. S., Parkinson H., 2008, *MNRAS*, 383, 546
- Eisenstein D.J., Loeb A., 1996, *MNRAS*, 459, 432
- Eisenstein D.J., Hu W., 1998, *ApJ*, 496, 605
- Fakhouri O., Ma C.-P., 2008, *MNRAS*, 386, 577
- Fakhouri O., Ma C.-P., 2009, *MNRAS*, 394, 1825
- Fakhouri O., Ma C.-P., Boylan-Kolchin M., 2010, *MNRAS*, 406, 2267 [F10]
- Gan J., Kang X., van den Bosch F.C., Hou J., 2010, *MNRAS*, 408, 2201
- Genel S., Genzel R., Bouche N., Sternberg A., Naab T., Schreiber N. M. F., Shapiro K. L., Tacconi L. J. et al., 2008, *ApJ*, 688, 789
- Genel S., Genzel R., Bouché N., Naab T., Sternberg A., 2009, *ApJ*, 701, 2002
- Genel S., Bouché N., Naab T., Sternberg A., Genzel R., 2010, *ApJ*, 719, 229 [G10]
- Giocoli C., Moreno J., Sheth R.K., Tormen G., 2007, *MNRAS*, 376, 977
- Giocoli C., Tormen G., van den Bosch F.C., 2008, *MNRAS*, 386, 2135 [G08]
- Han J., Jing Y.P., Wang H., Wang W., 2012, *MNRAS*, 427, 2437
- Harker G., Cole S., Helly J., Frenk C., Jenkins A., 2006, *MNRAS*, 367, 1039
- Helly J. C., Cole S., Frenk C.S., Baugh C.M., Benson A., Lacey C., 2003, *MNRAS*, 338, 903
- Hiotelis N., Del Popolo A., 2006, *Ap&SS*, 301, 167
- Jiang A.F., van den Bosch F.C., 2014, in preparation
- Kang X., Jing Y.P., Mo H.J., Börner G., 2005, *ApJ*, 631, 21
- Kauffmann G., White S.D.M., Guiderdoni B., 1993, *MNRAS*, 264, 201
- Kauffmann G., Colberg J.M., Diaferio A., White S.D.M., 1999, *MNRAS*, 303, 188
- Kauffmann G., Colberg J.M., Diaferio A., White S.D.M., 1999, *MNRAS*, 307, 529
- Lacey C., Cole S., 1993, *MNRAS*, 262, 627
- Li Y., Mo H.J., 2009, preprint (arXiv:0908.0301) [LM09]
- Lin W.P., Jing Y.P., Lin L., 2003, *MNRAS*, 344, 1327
- McBride J. Fakhouri O., Ma C.-P., 2009, *MNRAS*, 398, 1858
- Mo H., van den Bosch F.C., White S.D.M., 2010, *Galaxy Formation and Evolution*, Cambridge University Press
- Moreno J., Giocoli C., Sheth R.K., 2008, *MNRAS*, 391, 1729
- Neistein E., van den Bosch F.C., Dekel A., 2006, *MNRAS*, 372, 933
- Neistein E., Dekel A., 2008a, *MNRAS*, 388, 1792
- Neistein E., Dekel A., 2008b, *MNRAS*, 383, 615
- Nusser A., Sheth R.K., 1999, *MNRAS*, 303, 685
- Oguri M., Lee J., 2004, *MNRAS*, 355, 120
- Parkinson H., Cole S., Helly J., 2008, *MNRAS*, 383, 557 [P08]
- Purcell C.W., Zentner A.R., 2012, *JCAP*, 12, 007
- Sheth R.K., Lemson G., 1999, *MNRAS*, 305, 946
- Sheth R.K., Mo H.J., Tormen G., 2001, *MNRAS*, 323, 1
- Sheth R.K., Pitman J., 1997, *MNRAS*, 289, 66
- Sheth R.K., Tormen G., 2002, *MNRAS*, 329, 61
- Somerville R.S., Kolatt T.S., 1999, *MNRAS*, 305, 1 [SK99]
- Springel V., 2005, *MNRAS*, 364, 1105
- Srisawat C., Knebe A., Pearce F.R., Schneider A., Thomas P.A., Behroozi P., Dolag K., Elahi P.J., Han J., Helly J., preprint (arXiv:1307.3577)
- Taylor J.E., Babul A., 2005, *MNRAS*, 364, 515
- Taylor J.E., Babul A., 2005, *MNRAS*, 364, 535
- van den Bosch F.C., 2002, *MNRAS*, 331, 98
- van den Bosch F.C., Tormen G., Giocoli C., 2005, *MNRAS*, 359, 1029
- Wechsler R.H., Bullock J.S., Primack J.R., Kravtsov A.V., Dekel A., 2002, *ApJ*, 568, 52
- Wu H.-Y., Hahn O., Wechsler R.H., Mao Y.-Y., Behroozi P.S., 2013, *ApJ*, 763, 70
- Yang X., Mo H.J., Zhang Y., van den Bosch F.C., 2011, *ApJ*, 741, 13
- Zentner A.R., Bullock J.S., 2003, *ApJ*, 598, 49
- Zentner A.R., Berlind A.A., Bullock J.S., Kravtsov A.V., Wechsler R.H., 2005, *ApJ*, 624, 505
- Zhang J., Hui L., 2006, *ApJ*, 641, 641
- Zhang J., Ma C.-P., Fakhouri O., 2008, *MNRAS*, 387, L13
- Zhang J., Fakhouri O., Ma C.-P., 2008, *MNRAS*, 389, 1521 [Z08]
- Zhao D.H., Jing Y.P., Mo H.J., Börner G., 2009, *ApJ*, 707, 354